IEEE Photonics Journal
An IEEE Photonics Society Publication

Open Access

Simultaneous Measurement of the Refractive Index and Temperature Based on Microdisk Resonator With Two Whispering-Gallery Modes

Volume 9, Number 1, February 2017

Tao Ma
Jinhui Yuan
Lei Sun
Zhe Kang
Binbin Yan
Xinzhu Sang
Kuiru Wang
Qiang Wu
Heng Liu
Jinhui Gao
Chongxiu Yu

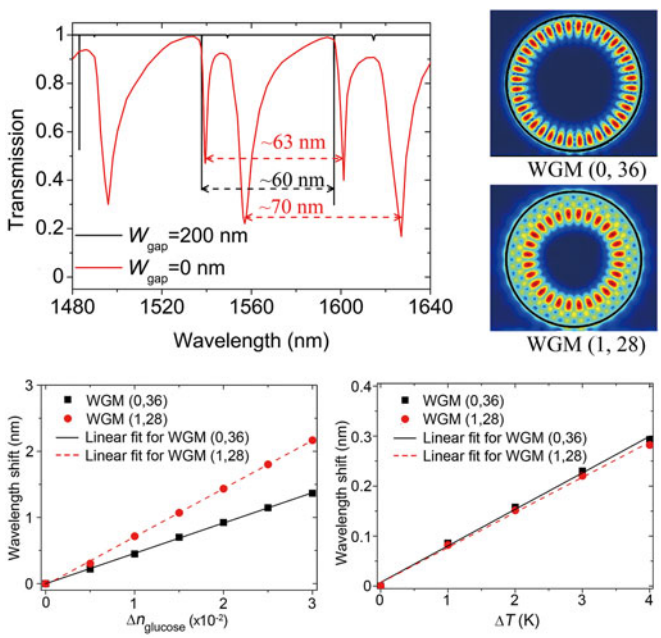

DOI: 10.1109/JPHOT.2017.2648259
1943-0655 © 2017 IEEE

Simultaneous Measurement of the Refractive Index and Temperature Based on Microdisk Resonator With Two Whispering-Gallery Modes

Tao Ma,[1,2] Jinhui Yuan,[1,3] Lei Sun,[1] Zhe Kang,[3] Binbin Yan,[1] Xinzhu Sang,[1] Kuiru Wang,[1] Qiang Wu,[4,5] Heng Liu,[2] Jinhui Gao,[2] and Chongxiu Yu[1]

[1]State Key Laboratory of Information Photonics and Optical Communications, Beijing University of Posts and Telecommunications, Beijing 100876, China
[2]College of Electronic and Electrical Engineering, Henan Normal University, Xinxiang 453002, China
[3]Photonics Research Centre, Department of Electronic and Information Engineering, Hong Kong Polytechnic University, Hung Hom, Hong Kong
[4]Photonics Research Centre, Dublin Institute of Technology, Dublin 8, Ireland
[5]Department of Electrical Engineering, Northumbria University, Newcastle Upon Tyne NE1 8ST, U.K.

DOI:10.1109/JPHOT.2017.2648259
1943-0655 © 2016 IEEE. Translations and content mining are permitted for academic research only. Personal use is also permitted, but republication/redistribution requires IEEE permission. See http://www.ieee.org/publications_standards/publications/rights/index.html for more information.

Manuscript received November 21, 2016; revised December 12, 2016; accepted December 28, 2016. Date of publication January 9, 2017; date of current version January 23, 2017. This work was supported in part by the National Natural Science Foundation of China under Grant 61307109 and Grant 61475023, in part by the Beijing Youth Top-notch Talent Support Program under Grant 2015000026833ZK08, in part by the Natural Science Foundation of Beijing under Grant 4152037, in part by the Fund of State Key Laboratory of Information Photonics and Optical Communications (BUPT) P. R. China under Grant IPOC2016ZT05, in part by the Hong Kong Scholars Program 2013 (PolyU G-YZ45), in part by the Key scientific and technological project of Henan province under Grant 132102210043, and in part by the Youth Scientific Funds of Henan Normal University under Grant 2011QK08 and Grant 2012QK08. Corresponding author: J. Yuan (e-mail: yuanjinhui81@163.com).

Abstract: In this paper, a microdisk resonator with two whispering-gallery modes (WGMs) is proposed for label-free biochemical sensing. According to the transmission responses of the two WGMs with different coupling gaps, there is the critical coupling status for the WGM (0, 36) while there is no critical coupling status for the WGM (1, 28). For the WGMs (0, 36) and (1, 28), the refractive index (RI) sensitivities of 45.8821 and 72.9402 nm/RIU are obtained, and the corresponding RI detection limits (DLs) of 8.5902×10^{-4} and 1.9228×10^{-3} RIU are achieved, respectively. Moreover, the proposed sensor also has the temperature sensitivities of 0.0730 and 0.0703 nm/K, which correspond to the temperature DLs of 0.1631 and 0.6263 K, respectively. By constructing a characteristic matrix, it is demonstrated that simultaneous measurement of the RI and temperature can be achieved.

Index Terms: Microdisk resonator, whispering-gallery mode, refractive index (RI), temperature.

1. Introduction

Label-free biomedical sensors can provide real-time quantitative information on the progress of the biochemical reaction. In particular, optical micro-resonators based on silicon-on-insulator (SOI) have attractive characteristics for label-free sensing applications. Compared with the sensors based

on straight waveguide, the sensors based on micro-resonators have a reduced size but without reducing detection limit (*DL*) due to the high quality (*Q*) factor of micro-resonators. In addition, the micro-resonators based biochemical sensors have interesting advantages including high sensitivity, compactness, simple fabrication, surface functionalization, and multiplexing analysis capability. Different micro-resonators, such as microring [1], microdisk [2], micro-racetrack [3], and microsphere [4], have been utilized for label-free sensing applications. Among the reported micro-resonator structures, microdisk resonators have attracted great attention because of their potential sensing applications and easy fabrication [5].

As demonstrated in previous works [6], the micro-resonators based on SOI have a vulnerability to the temperature change. Moreover, the high thermo-optic coefficient of silicon and the wavelength selectivity of micro-resonators make them susceptible to the temperature fluctuation. Due to the sensitivity to the temperature, the micro-resonators can be proposed as the temperature sensors [7]–[9], but the sensitivity to the temperature is a disadvantage for some other optical devices, for example, the refractive index (RI) sensors based on the micro-resonator.

In order to eliminate the temperature effect, the sensing schemes [10], [11] have been proposed by introducing a reference microring. Another sensing scheme, where a ring resonator is combined with a Mach-Zehnder interferometer [12], [13], have been also used to eliminate the influence of environment temperature. Besides, dual-microring scheme with resonance splitting [14] has been employed to reduce the temperature dependence of the micro-resonators. However, these additional reference configurations increase the size of the devices, which are not beneficial to the device integration. In addition, the temperature control devices [15], [16] used for temperature compensation require the integrated heaters and photodetectors, which give rise to the power consumption.

At present, some materials with negative thermal-optic coefficients (TOCs) [17]–[21] are used for compensating the positive TOCs of sensing devices, but it requires to precisely control the thickness of the negative TOCs layer. Measurement of temperature during the sensing process is another approach to remove the temperature influence. Microring resonators with dual polarization or two WGMs are proposed for simultaneous measurement of the refractive index (RI) and temperature [22], [23]. However, these proposed microrings with a big radius ($>$20 μm) increase the device size and reduce the free spectral range (FSR). Recently, a single wavelength reflective microring along with a distributed Bragg reflector (DBR) [24] is designed to measure the RI and TOC of the waveguide core (silicon nitride) and cladding (silica). However, it is not used as a sensor for simultaneous measurement of the surrounding RI and temperature. Surface plasmon polaritons (SPPs) refractive index sensor based on metal-insulator-metal (MIM) waveguides [25] for measuring the surrounding RI and temperature are demonstrated. This sensor can obtain very high sensitivities (S), but the *Q* factor and *DL* are low due to the ohmic loss of metal materials.

In this paper, an optical microdisk resonator with two WGM resonance peaks is proposed to measure the changes of the surrounding RI and temperature simultaneously. The mode characteristics and transmission responses of the two WGMs are simulated by the 3-D finite element method (3D-FEM). *Q* factor and extinction ratio (*ER*) of the two WGM resonance peaks are studied with different coupling media and gaps. Manufacturing tolerances of the microdisk resonator are also discussed to demonstrate the accuracy and stability of the proposed sensor. For the sensing performances, both the RI and temperature changes can be obtained by simultaneously measuring the resonance wavelength shifts of the two WGMs.

2. Theoretical Model and Analysis

Fig. 1 shows the schematic diagram of the microdisk resonator and the cross-section at the input port. The SOI wafer is used as the waveguide material where a 220 nm Si layer ($n_{Si} = 3.48$) is the device layer on a 2 μm SiO_2 insulator layer ($n_{SiO_2} = 1.44$) along with the air cladding ($n_c = 1$). Structural parameters of the microdisk resonator are labelled in Fig. 1. The radius (*R*) of the microdisk resonator is 2 μm. W_{gap} is the coupling gap between the bus waveguide and the microdisk resonator. The bus waveguide width and thickness are labelled as *w* and *h*, respectively. Here, *h*

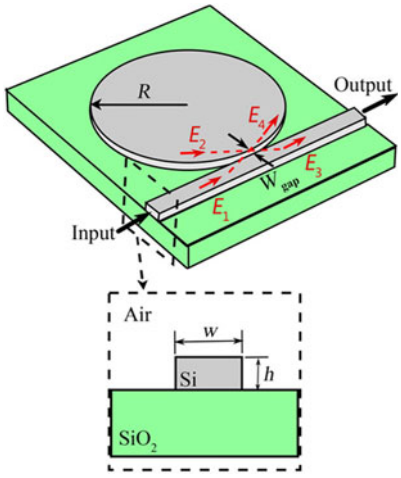

Fig. 1. Schematic of a microdisk resonator based on SOI and the cross-section of the bus waveguide at the input port.

is 220 nm, and W_{gap} and w are optimized. Accoring to the radius of the microdisk resonator, the device dimension is about 5 μm × 5 μm.

As shown in Fig. 1, the coupling light between the bus waveguide and microdisk resonator can be described as [26]

$$\begin{cases} E_3 = \tau E_1 + \mathrm{i}kE_2 \\ E_4 = \mathrm{i}kE_1 + \tau E_2 \end{cases} \tag{1}$$

where τ and k are the amplitude coefficient of transmission field and the coupling coefficient between the microdisk and bus waveguide, respectively. For the lossless coupling condition, $\tau^2 + k^2 = 1$. The electric field amplitudes E_j ($j = 1, 2, 3, 4$) are defined with respect to the red arrow positions, as shown in Fig. 1. E_4 can be described as

$$E_4 = \alpha \mathrm{e}^{\mathrm{i}\varphi} E_2 \tag{2}$$

where α and φ are the amplitude transmission coefficient and the phase shift with a single round trip along the microdisk. From (1) and (2), the intensity transmission factor can be given as

$$T = \left|\frac{E_3}{E_1}\right|^2 = \frac{\tau^2 - 2r\tau\cos\varphi + \alpha^2}{1 - 2\alpha\tau\cos\varphi + \alpha^2\tau^2}. \tag{3}$$

The 3D-FEM is used to simulate the propagation characteristics and the sensing performance of the micodisk resonator. The mode at the input port is calculated by analyzing the boundary mode which is injected into the bus waveguide. Subsequently, the WGMs in microdisk are also achieved by frequency domain analysis method. The intensity transmission factor of microdisk can be calculated by using S_{21}

$$S_{21}(\mathrm{dB}) = 10\lg\left(\frac{P_o}{P_i}\right) \tag{4}$$

where P_i and P_o are the powers at the input and output ports of the bus waveguide, respectively.

3. Performance of the Microdisk Resonator

3.1. Mode Characteristics

The effective refractive indices of different modes, which are supported in the bus waveguide, are calculated as functions of w, as shown in Fig. 2. Here, the wavelength is set as 1550 nm.

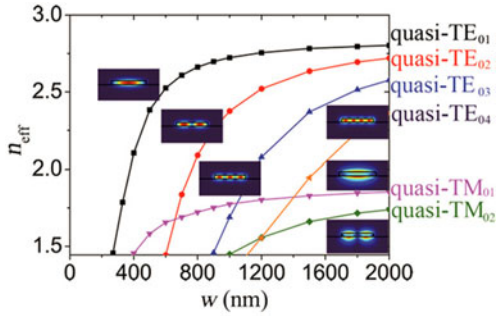

Fig. 2. Effective refractive indices of the supported modes in the bus waveguide as functions of *w*, the insets showing the corresponding mode distributions.

The number of modes in the bus waveguide increases when *w* increases. In order to ensure the single-mode propagation (only quasi-TE_{01}), *w* is chosen as 400 nm. The corresponding mode distributions are also shown in the insets of Fig. 2.

3.2. Transmission Responses

With the injection of quasi-TE_{01} at the input port of the bus waveguide, the transmission spectra with different W_{gap} are shown in Fig. 3(a). According to the coupled-mode theory (CMT) [27] and hybrid coupled mode theory (HCMT) [28], there are only two lowest WGMs supported in the proposed microdisk resonator with small radii of 5 and 7.5 μm, respectively. Here, the radius of the designed microdisk is chosen as 2 μm for only two lowest WGMs supported in the microdisk resonator. The transmission spectra with W_{gap} of 0 and 200 nm within the wavelength range from 1480 to 1640 nm are shown in Fig. 3(b). For W_{gap} of 200 nm, there is only one group of dominated WGMs, and their FSR is ~60 nm. However, there are two groups of remarkable WGMs for W_{gap} of 0 nm, and their corresponding FSRs are ~63 and ~70 nm, respectively. A notation WGM (*l*, *m*) [28] is used to characterize the WGMs, and *l* and *m* are the number of radial minima and angular wavenumber, respectively. Hence, the two WGMs in the microdisk resonator can be represented by the WGM (0, 36) at the wavelength of ~1537 nm and WGM (1, 28) at the wavelength of ~1550 nm, and the corresponding mode distributions are shown in Fig. 3(c) and (d), respectively.

For sensing application, *S* and *DL* are the main parameters for evaluating the sensing capability of the device. In order to enhance *S* and *DL*, it is necessary to investigate *Q* factor and *ER*. *Q* factor can be calculated as the ratio of resonance wavelength (λ_0) and full width at half maximum (FWHM) of the resonant peak in the transmission spectrum [29]

$$Q = \frac{\lambda_0}{\text{FWHM}}. \tag{5}$$

ER is defined as [30]

$$ER = -10 \lg \left(\frac{P_o}{P_i} \right). \tag{6}$$

The coupling loss induced is a main factor which affects the *Q* factor. The coupling loss is greatly dependent on W_{gap}. The dependences of *Q* factor and *ER* of the resonance peaks at the WGM (0, 36) and WGM (1, 28) on W_{gap} are shown in Fig. 3(e) and (f), respectively. For the WGM (0, 36), the changes of *Q* factor and *ER* with the increase of W_{gap} are similar to those of the conventional microring. There is a critical coupling status when W_{gap} is ~120 nm. *Q* factor monotonically increases with the increase of W_{gap} from 0 to 300 nm. However, *ER* firstly increases to the maximum value at W_{gap} of ~120 nm and then decreases. In general, high *Q* factor resonators are beneficial to reduce the spectral noise of the sensor and improve *DL*. Therefore, W_{gap} of 200 nm is chosen for higher *Q* factor (~8×10^4), and the corresponding *ER* is ~4.50 dB. For the WGM (1, 28), there is

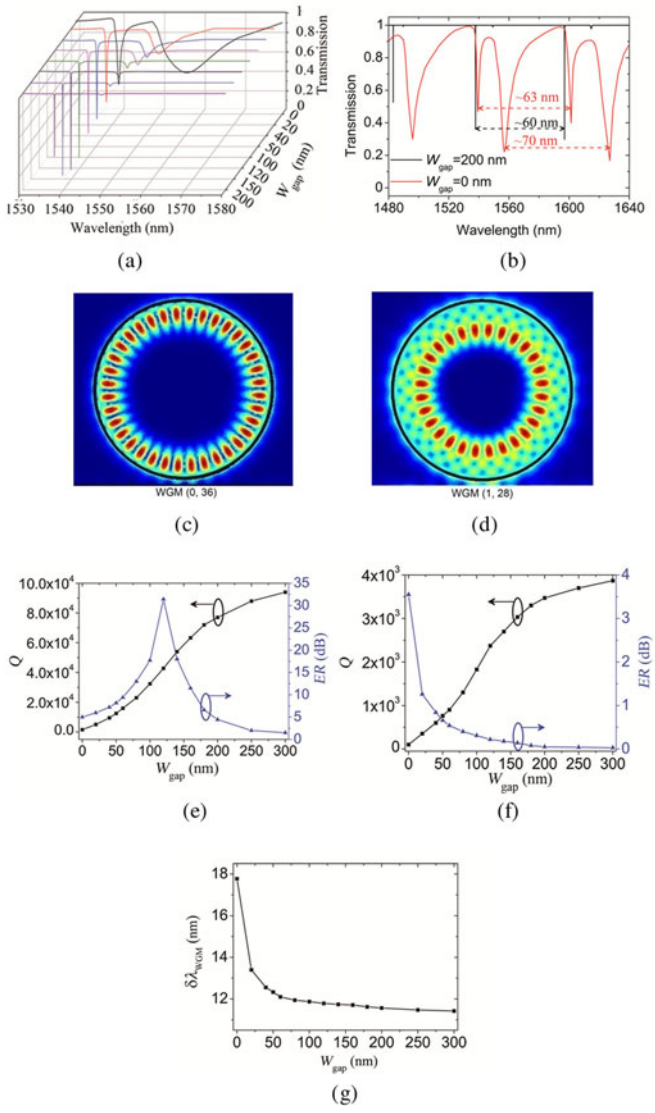

Fig. 3. (a) Transmission spectra of the microdisk resonator with different W_{gap}, (b) transmission spectra with W_{gap} of 0 and 200 nm within the wavelength range from 1480 to 1640 nm, field distributions of (c) WGM (0, 36) and (d) WGM (1, 28), and Q factor and ER of (e) WGM (0, 36) at ~1537 nm and (f) WGM (1, 28) at ~1550 nm as a function of W_{gap}, and (g) resonance wavelength difference $\delta\lambda_{WGM}$ between the two WGMs as a function of W_{gap}.

not the critical coupling status. Q factor monotonically increases with the increase of W_{gap}, and ER monotonically decreases. As seen from Fig. 3(f), there is a trade-off between Q and ER. A larger W_{gap} will result in higher Q factor but smaller ER. The resonance wavelength difference $\delta\lambda_{WGM}$ between the two WGMs as a function of W_{gap} is also shown in Fig. 3(g). With the increase of W_{gap}, $\delta\lambda_{WGM}$ decreases sharply when W_{gap} is close to 0 nm and then changes slowly.

Because most of the biochemical analytes are the aqueous solutions, it is necessary to evaluate the transmission characteristics of the microdisk resonator with the water cladding ($n_c = 1.33$) instead of the air one. Comparing with the air cladding, the water cladding results in the increase of the effective RI of the waveguide. Then, the resonant wavelength of the micodisk resonator has a red-shift for both the WGM (0, 36) and WGM (1, 28). Q factor and ER of the microdisk resonator with the air and water cladding are presented in Fig. 4. With W_{gap} of 200 nm, Q factor and ER of

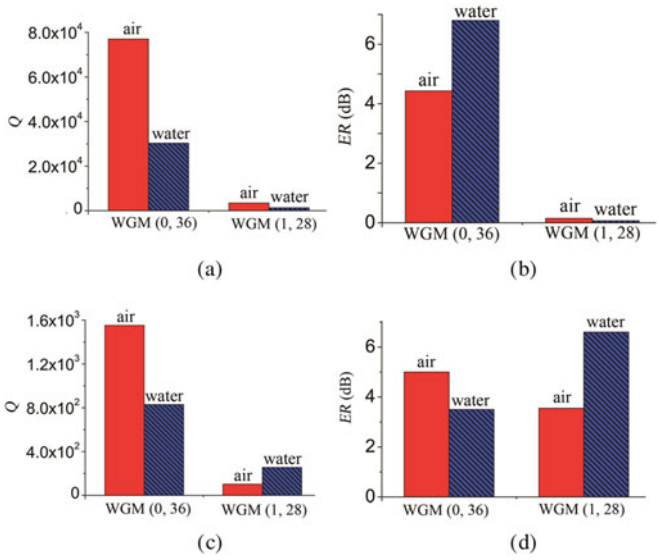

Fig. 4. (a) *Q* factor and (b) *ER* of the microdisk resonator with the air and water cladding for W_{gap} of 200 nm. (c) *Q* factor and (d) *ER* of the microdisk resonator with the air and water cladding for W_{gap} of 0 nm.

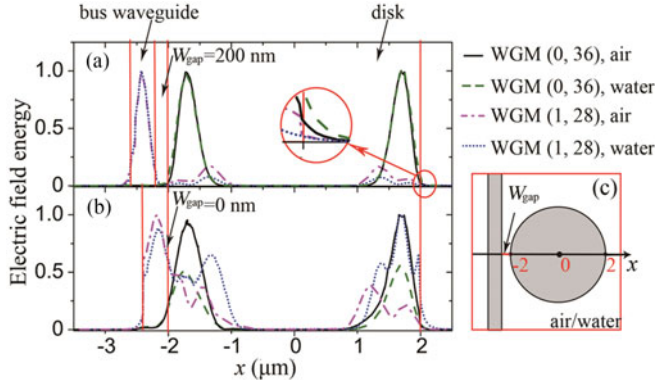

Fig. 5. Normalized electric field energy along the *x* axis of the micordisk resonator for (a) W_{gap} of 200 nm and (b) W_{gap} of 0 nm. (c) Top view of the proposed microdisk resonator.

the microdisk resonator with the air and water cladding are shown in Fig. 4(a) and (b), respectively. For the water cladding, *Q* factors of the two WGMs decrease. However, *ER* increases for the WGM (0, 36) and decrease for the WGM (1, 28). As shown in Fig. 4(b), the resonance peak of the WGM (0, 36) is the dominant peak in the microdisk resonator. With W_{gap} of 0 nm, *Q* factor and *ER* of the microdisk resonator with the air and water cladding are shown in Fig. 4(c) and (d), respectively. It can be seen from Fig. 4(c) and (d) that *Q* factor and *ER* of the microdisk resonator with the water cladding decrease for the WGM (0, 36) but increase for the WGM (1, 28). The resonance peak of the WGM (1, 28) can be compared to that of the WGM (0, 36), as shown in Fig. 4(d).

In order to investigate the change of *Q* factors in Fig. 4, the normalized electric field energy along the *x* axis are shown in Fig. 5(a) and (b). The top view of the proposed microdisk resonator is shown in Fig. 5(c). As seen from Fig. 5(a), for W_{gap} of 200 nm, *Q* factor of the WGM (0, 36) with the water cladding decreases compared to that with the air cladding due to the increasing of the radiation energy as shown in the inset of Fig. 5(a). *Q* factor of the WGM (1, 28) with the water cladding decreases compared to that with the air cladding because the stored energy in the microdisk resonator decreases. As shown in Fig. 5(b), for W_{gap} of 0 nm, *Q* factor of the WGM (0, 36) with the

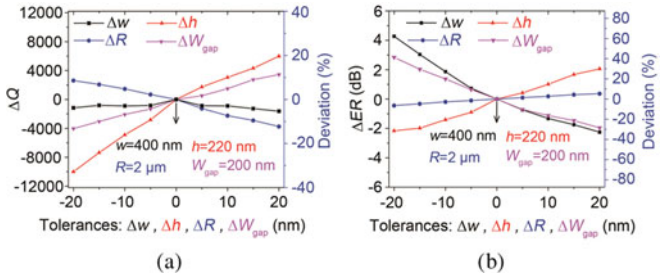

Fig. 6. Effects of structure dimensional deviations of the microdisk resonator on its performance. (a) ΔQ and deviation in % from the calculated nominal value of 3.05×10^4 for the WGM (0, 36) and (b) ΔER and deviation in % from the calculated nominal value of 6.87 dB for the WGM (0, 36). Both graphs are plotted over the tolerances of Δw, Δh, ΔR, and ΔW_{gap}.

water cladding decreases due to the decreasing of the stored energy in the microdisk resonator. However, for the WGM (1, 28), *Q* factor still increases even if the radiation energy increases because the stored energy is increased more than the radiation energy.

3.3. Manufacturing Tolerance

In order to study the accuracy and stability of the proposed microdisk, it is necessary to discuss the effects of the structure dimensional deviations on the performance of the microdisk resonator. The effects of waveguide profile angle and surface roughness on the performance of micro-resonators have already been discussed [31]–[33]. Here, the influence of the deviations of *w*, *h*, *R*, and W_{gap} on *Q* factor and *ER* of the microdisk resonator will be demonstrated. The specific structural parameters *w* of 400 nm, *h* of 220 nm, and *R* of 2 μm are chosen. Meanwhile, the dimensional deviations are changed from −20 to +20 nm [34]. For W_{gap} of 200 nm, the effect of WGM (1, 28) on the transmission characteristic can be neglected because its *ER* is much smaller than that of the WGM (0, 36), as shown in Fig. 4(b). The cladding RI is set as 1.33. Then the calculated nominal values of *Q* factor and *ER* are $\sim 3.05 \times 10^4$ and 6.87 dB for the WGM (0, 36), respectively. The simulation results are shown in Fig. 6(a) and (b), respectively. ΔQ and ΔER are the changes of *Q* factor and *ER*, which vary with the structure dimensional deviations (Δw, Δh, ΔR, and ΔW_{gap}). The relative deviations from the nominal values in % are also shown in Fig. 6(a) and (b). Here, *Q* factor of the microdisk resonator is very stable with respect to the change of Δw compared to the other structure dimensional deviations. Meanwhile, the effect of ΔR on *ER* is less than the other tolerances. Both *Q* factor and *ER* are greatly affected by the variation of Δh.

For $W_{gap} = 0$ nm, it is necessary to discuss the effect of the WGM (1, 28) on the transmission characteristic because its *ER* becomes comparable to that of the WGM (0, 36), as shown in Fig. 4(d). The nominal values of *Q* factor and *ER* are calculated as $\sim 1.02 \times 10^3$ and 3.21 dB for the WGM (0, 36), and 268.58 and 6.25 dB for the WGM (1, 28), respectively. The effects of dimensional deviations of the microdisk resonator on its performance for the WGM (0, 36) and WGM (1, 28) are shown in Figs. 7 and 8, respectively. From Figs. 7(a) and 8(a), *Q* factor increases sharply by a maximum of 90% with positive change of the coupling gap change ΔW_{gap}, which is much bigger than the other tolerances. However, for the negative changes of ΔW_{gap}, *Q* factor change slowly. It can be seen from Figs. 7(b) and 8(b) that *ER* is significantly influenced by Δw and ΔW_{gap} compared to the other two tolerances.

From the analysis above, it is known that the effect of structure dimensional deviations during the fabrication process plays an important role in the performances of the SOI microdisk resonator. In order to reduce the effect of structure dimensional deviations, it is necessary to improve the precision of the fabrication process. By using the micro-nano manufacturing technology, the precision can be improved to a few nanometres. In addition, the simulation results for deviations in *Q* factor and *ER* indicate that the different tolerances could compensate each other.

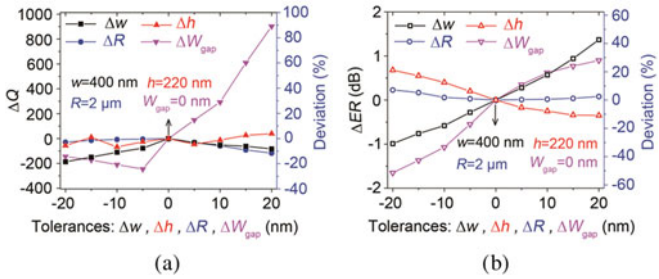

Fig. 7. Effects of structure dimensional deviations of the microdisk resonator on its performance for the WGM (0, 36). (a) ΔQ and deviation in % from the calculated nominal value of 1.02×10^4 and (b) ΔER and deviation in % from the calculated nominal value of 3.21 dB. Both graphs are plotted over the tolerances of Δw, Δh, ΔR, and ΔW_{gap}.

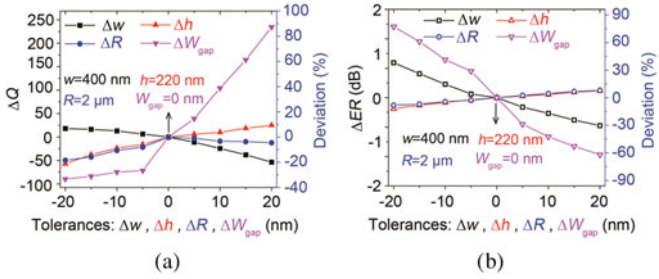

Fig. 8. Effects of structure dimensional deviations of the microdisk resonator on its performance for the WGM (1, 28). (a) ΔQ and deviation in % from the calculated nominal value of 268.58 and (b) ΔER and deviation in % from the calculated nominal value of 6.25 dB. Both graphs are plotted over the tolerances of Δw, Δh, ΔR, and ΔW_{gap}.

4. Sensing Performance

The microdisk resonator can be used for the biochemical sensing by measuring the surrounding RI change which is induced by biological material and/or chemical concentration changes. The optical field of the mcirodisk resonator interacts with the surrounding analytes, and then the resonance wavelength shift can be obtained with the read-out system. Here, the RI sensitivity (S_n) and temperature sensitivity (S_T) are respectively defined as the resonant wavelength shift ($\Delta\lambda_{\text{res}}$) versus the RI change ($\Delta n_c$) and temperature change (ΔT) of the analytes detected [30]

$$S_n = \frac{\Delta\lambda}{\Delta n_c} \text{ and } S_T = \frac{\Delta\lambda}{\Delta T}. \tag{7}$$

The *DL* characterizes the smallest change of the RI, which can be described as [35]

$$DL = \frac{R_\sigma}{S} = \frac{3\sigma}{S} = \frac{3\text{FWHM}}{4.5(SNR)^{0.25}S} \tag{8}$$

where R_σ is the sensor resolution which describes the measurable smallest spectral shift, σ is the standard deviation of the total noise of the system, and SNR is the signal-noise ratio for sensor system and considered as the linear units (*e.g.*, 60 dB = 10^6). The SNR of 60 dB is good for a typical photonic link.

First, the wavelength shift of the WGM (0, 36) resonant peak with W_{gap} of 200 nm is used for the RI sensing. In the following, the microdisk resonator based sensor is covered by the solutions with different concentrations instead of the air. For example, the RIs of sodium chloride and cell solutions with different concentrations are changed from 1.33 to 1.4. Thus, n_c is chosen from 1.33 to 1.4 with a step of 0.01. The transmission spectra of the mcirodisk resonator in response to n_c

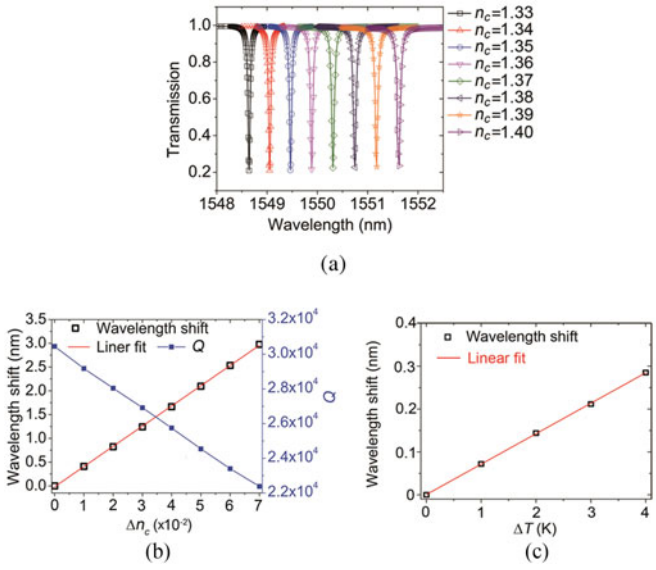

Fig. 9. (a) Transmission spectra of the sensor with different n_c from 1.33 to 1.4 with a step of 0.01 using the WGM (0, 36) resonance peak and wavelength shift and Q factor as functions of (b) Δn_c and (c) ΔT. The red-solid lines are the linear fits of the wavelength shift.

are shown in Fig. 9(a). By using the Lorentz fits of the transmission spectra, the calculated Q of the microdisk resonator with different n_c is shown in Fig. 9(b). and Q decreases with the increase of Δn_c. The wavelength shifts with the increasing of Δn_c and the corresponding linear fit are also shown in Fig. 9(b). It can be seen that the resonance wavelength shifts toward the longer wavelength side with the increasing of n_c. The slope and its standard error (*SE*) of the fitted line is 42.5211 and 0.2267 nm/RIU, respectively. The SE is the standard deviation of the sampling distribution of a statistic based on the wavelength shifts with different Δn_c. The slope of the linear fit is the RI sensitivity of the proposed sensor. For a *SE* of 0.0006 nm, λ_{FWHM} of 0.0509 nm can be achieved from the transmission spectrum at n_c of 1.33. According to (8), the RI *DL* of 2.5236×10^{-5} RIU can be achieved.

In order to simulate the temperature influence on the sensing performance, the TOCs are used to calculate the RI changes of waveguides caused by the temperature change. At temperature of 295 K and wavelength of 1550 nm, the TOCs of Si, SiO_2, and water are about 1.8×10^{-4}/K, 2.8×10^{-5}/K, and -9.9×10^{-5}/K, respectively [36]. Fig. 9(c) shows the wavelength shift of the WGM (0, 36) resonant peak as a function of ΔT when the waveguide cladding is the pure water. According to the linear fit, S_T is 0.0710 nm/K with a *SE* of 0.0004 nm/K, and the temperature *DL* of 0.1511 K can be achieved.

Subsequently, both the WGM (0, 36) and WGM (1, 28) are considered for simultaneous measurement of the RI and temperature. W_{gap} is set as 0 nm for the trade-off of *ER* between the WGM (0, 36) and WGM (1, 28), as shown in Fig. 4. Here, the aqueous solutions of D-Glucose in pure water with various concentrations (0∼0.2 g/ml) are used as the analyte. The RIs of the glucose solutions can be estimated as [37]

$$n_{glucose} = n_{H_2O} + 1.515 c_{glucose} \tag{9}$$

where $n_{glucose}$ and n_{H_2O} are the RIs of the glucose solution and pure water, respectively. $c_{glucose}$ is the concentration of glucose solution in g/ml. The cladding RI is set as $n_{glucose}$ instead of n_c, and $\Delta n_{glucose}$ is the RI change of the glucose solutions from the pure water. The wavelength shifts as functions of $\Delta n_{glucose}$ for the two WGMs and their linear fits are shown in Fig. 10(a). S_{n1} of 45.8821 nm/RIU with a *SE* of 0.3754 nm/RIU and S_{n2} of 72.9402 nm/RIU with a *SE* of 0.7685 nm/RIU for the WGM

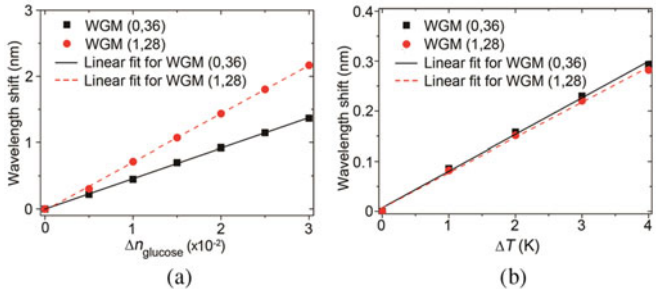

Fig. 10. Wavelength shifts as functions of (a) $\Delta n_{\text{glucose}}$ and (b) ΔT for the WGM (0, 36) and WGM (1, 28). The black-solid and red-dash lines are the linear fits of wavelength shift for the WGM (0, 36) and WGM (1, 28), respectively.

(0, 36) and WGM (1, 28) can be obtained, respectively. The corresponding RI *DL* of 8.5906×10^{-4} and 1.9228×10^{-3} RIU can be achieved. At a fixed temperature ($\Delta T = 0$), the wavelength shifts $\Delta\lambda_{\text{WGM (0, 36)}}$ for the WGM (0, 36) and $\Delta\lambda_{\text{WGM (1, 28)}}$ for the WGM (1, 28) as functions of the $\Delta n_{\text{glucose}}$ can be given by

$$\begin{cases} \Delta\lambda_{\text{WGM (0, 36)}}\big|_{\Delta T=0} = S_{n1}\Delta n_{\text{glucose}} \\ \Delta\lambda_{\text{WGM (1, 28)}}\big|_{\Delta T=0} = S_{n2}\Delta n_{\text{glucose}} \end{cases}. \tag{10}$$

Finally, the temperature measurements by using the two WGMs are also investigated. Fig. 9(b) shows $\Delta\lambda_{\text{WGM (0, 36)}}$ and $\Delta\lambda_{\text{WGM (1, 28)}}$ as functions of the temperature variations when the waveguide cladding is water. According to the linear fits, S_{T1} of 0.0730 nm/K with a *SE* of 0.0022 nm/K and S_{T2} of 0.0703 nm/K with a *SE* of 0.0021 nm/K are achieved for the WGM (0, 36) and WGM (1, 28), respectively. The corresponding temperature *DL* of 0.1631 and 0.6263 K can be achieved. When there is an ambient temperature change ΔT at a fixed solution RI ($\Delta n_{\text{glucose}} = 0$), $\Delta\lambda_{\text{WGM (0, 36)}}$ and $\Delta\lambda_{\text{WGM (1, 28)}}$ can be obtained as

$$\begin{cases} \Delta\lambda_{\text{WGM (0, 36)}}\big|_{\Delta n_{\text{glucose}}=0} = S_{T1}\Delta T \\ \Delta\lambda_{\text{WGM (1, 28)}}\big|_{\Delta n_{\text{glucose}}=0} = S_{T2}\Delta T \end{cases}. \tag{11}$$

According to the (10) and (11), $\Delta\lambda_{\text{WGM (0, 36)}}$ and $\Delta\lambda_{\text{WGM (1, 28)}}$ induced by the changes of the RI and temperature simultaneously can be described by

$$\begin{aligned} \begin{bmatrix} \Delta\lambda_{\text{WGM (0, 36)}} \\ \Delta\lambda_{\text{WGM (1, 28)}} \end{bmatrix} &= \mathbf{M}_{n,T} \begin{bmatrix} \Delta n_{\text{glucose}} \\ \Delta T \end{bmatrix} = \begin{pmatrix} S_{n1} & S_{T1} \\ S_{n2} & S_{T2} \end{pmatrix} \begin{bmatrix} \Delta n_{\text{glucose}} \\ \Delta T \end{bmatrix} \\ &= \begin{pmatrix} 45.8821 & 0.0730 \\ 72.9402 & 0.0703 \end{pmatrix} \begin{bmatrix} \Delta n_{\text{glucose}} \\ \Delta T \end{bmatrix} \end{aligned} \tag{12}$$

where $\mathbf{M}_{n,T}$ [22], [23] is defined as a characteristic matrix to represent the sensing performance of the two WGMs. Since the wavelength shifts of $\lambda_{\text{WGM (0, 36)}}$ and $\lambda_{\text{WGM (1, 28)}}$ can be independently measured, the RI and temperature changes can be simultaneously measured by monitoring the resonance shifts of the two WGMs as

$$\begin{aligned} \begin{bmatrix} \Delta n_{\text{glucose}} \\ \Delta T \end{bmatrix} &= \mathbf{M}_{n,T}^{-1} \begin{bmatrix} \Delta\lambda_{\text{WGM (0, 36)}} \\ \Delta\lambda_{\text{WGM (1, 28)}} \end{bmatrix} \\ &= \begin{pmatrix} -0.0335 & 34.7479 \\ 0.0348 & -21.8577 \end{pmatrix} \begin{bmatrix} \Delta\lambda_{\text{WGM (0, 36)}} \\ \Delta\lambda_{\text{WGM (1, 28)}} \end{bmatrix} \end{aligned} \tag{13}$$

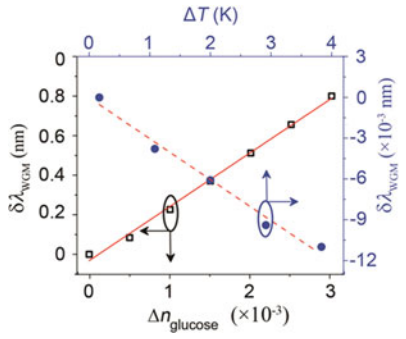

Fig. 11. Resonance wavelength difference between the two WGMs ($\delta\lambda_{WGM}$) as functions of $\Delta n_{glucose}$ and ΔT. The red-solid and dash lines are the linear fits of $\delta\lambda_{WGM}$ with different $\Delta n_{glucose}$ and ΔT, respectively.

TABLE 1

Comparisons of Sensing Performance of Several Optical Micro-Resonators

Optical resonator	Variables	Radius (μm)	Modes	Wavelength width between two modes (nm)	S_n (nm/RIU)	DL of RI (RIU)	S_T (pm/K)	DL of temperature (K)	Ref.
microring (SOI)	RI, Temperature	50	WGM (1, 569)	~20 nm	2.9	$\sim 10^{-7}$	3.5	$\sim 10^{-3}$	22
			WGM (2, 550)		29		1.0	5.6×10^{-3}	
		166	WGM (36, 707)		147.9	2.2×10^{-5}	−6.9		
			WGM (37, 700)		636.1		−56.9		
Microring (SOI)	RI, Temperature	20	WGMs (TE_0)	~1.5 nm	104	1.2×10^{-4}	78.7	0.5	23
			WGMs (TM_0)		319	3.8×10^{-4}	34.1	1.1	
DBR microring (Si_3N_4/SiO_2)	RI, TOC	30	WGMs (TE)	–	316	–	16.81	-	24
		46.7			578		14.55	-	
			WGMs (TM)		265	-	16.47	-	
			WGMs (TE)		545	-	13.99	-	
			WGMs (TM)			-			
micoring (MIM)	RI, Temperature	0.17	surface plasmon polaritons (SPPs)	~800 nm	732.92	-	290	-	25
					1476.25		580	-	
microdisk (SOI)	RI, Temperature	2	WGM (0, 36)	~18 nm	45.8821	8.5906×10^{-4}	73.0	0.1631	our work
			WGM (1, 28)		72.9402	1.9228×10^{-3}	70.3	0.6263	

The resonance wavelength differences ($\delta\lambda_{WGM}$) between the two WGMs with different $\Delta n_{glucose}$ and ΔT and their linear fits are shown in Fig. 11. $\delta\lambda_{WGM}$ increases at a rate of ~27.3604 nm/RIU (with a *SE* of 0.7316 nm/RIU) with the increase of $\Delta n_{glucose}$, and decreases at a rate of 0.0028 nm/K (with a *SE* of 0.0002 nm/K) with the increase of ΔT. The RI sensitivity is less than that (45.8821 or 72.9402 nm/RIU) by monitoring the wavelength shift of a single WGM and is close to the experi-

ment one (20 nm/RIU) of the WGMs-based sensor in [38]. The temperature sensitivity by monitoring $\delta\lambda_{WGM}$ is about one 26th of that by monitoring the wavelength shift of the WGM (0, 36) or WGM (1, 28). Hence, $\delta\lambda_{WGM}$ affected by temperature is much less than $n_{glucose}$ compared with the wavelength shift of a single WGM. By monitoring $\delta\lambda_{WGM}$, the measurement of RI can be achieved with less temperature influence with the compromising RI sensitivity.

In Table 1, comparisons of the sensing performance of several optical micro-resonators for simultaneous measurement of the RI and temperature are given. The operating wavelengths are considered within the visible or near-infrared spectral regions. From Table 1, the proposed microdisk resonator in our work has smaller radius except for that demonstrated in [25]. Due to the smaller radius, a wider FSR can be achieved to enlarge the measurement range [39]. In the case of silicon photonics, low-loss waveguides ($<$1 dB/cm) have been demonstrated at the wavelength of 1550 nm [40] for a small radius. Meanwhile, the small device size is easy of integration on a chip for applications of portable instruments. It can also be seen from Table 1 that the wavelength interval between the two WGMs in our work of $\sim$18 nm is much smaller than that of the microring based on MIM, which can effectively reduce the wavelength scanning range. Moreover, compared to [22]–[24], the proposed microdisk resonator has higher temperature sensitivity of 0.0730 nm/K and lower temperature *DL* of 0.1631 K for the two WGMs used.

5. Conclusion

In conclusion, simultaneous measurement of surrounding RI and temperature changes can be achieved by using two WGMs. The transmission responses of the WGM (1, 28) and WGM (0,36) with different W_{gap} indicate their different coupling status. The RI and temperature sensing performances by monitoring the resonance wavelengths of a single WGM and two WGMs are investigated. The results show that the RI sensitivity by only monitoring the resonance wavelength shift of the WGM (1, 28) is 72.9402 nm/RIU, which is higher than that (42.5211 or 45.8821 nm/RIU for different W_{gap}) of the WGM (0, 36). However, the approximate temperature sensitivities of 0.0730 and 0.0703 nm/K for WGM (0, 36) and WGM (1, 28) are respectively achieved by monitoring different WGMs. Thus, the RI and temperature changes are simultaneously measured by monitoring the resonance shifts of the two WGMs with a character matrix. In other words, the measurement of RI with less temperature influence is achieved by monitoring $\delta\lambda_{WGM}$ with the compromising RI sensitivity. The proposed sensor has a potential application in simultaneous measurement of multi-variables, such as RI, temperature, humidity, stress, etc., by using more WGMs and is easy to integrate with other SOI devices.

References

[1] D. X. Xu *et al.*, "Real-time cancellation of temperature induced resonance shifts in SOI wire waveguide ring resonator label-free biosensor arrays," *Opt. Exp.*, vol. 18, no. 22, pp. 22867–22879, Oct. 2010.
[2] R. W. Boyd and J. E. Heebner, "Sensitive disk resonator photonic biosensor," *Appl. Opt.*, vol. 40, no. 31, pp. 5742–5747, Nov. 2001.
[3] V. K. De, I. Bartolozzi, E. Schacht, P. Bienstman, and R. Baets, "Silicon-on-Insulator microring resonator for sensitive and label-free biosensing," *Opt. Exp.*, vol. 15, no. 12, pp. 7610–7615, Jun. 2007.
[4] N. M. Hanumegowda, C. J. Stica, B. C. Patel, I. White, and X. Fan, "Refractometric sensors based on microsphere resonators," *Appl. Phys. Lett.*, vol. 87, no. 20, Nov. 2005, Art. no. 201107.
[5] A. N. Oraevsky, "Whispering-gallery waves," *Quantum Electron.*, vol. 32, no. 5, pp. 377–400, 2002.
[6] M. S. Nawrocka, T. Liu, X. Wang, and R. R. Panepucci, "Tunable silicon microring resonator with wide free spectral range," *Appl. Phys. Lett.*, vol. 89, no. 7, Aug. 2006, Art. no. 71110.
[7] C. T. Wang *et al.*, "Highly sensitive optical temperature sensor based on a SiN micro-ring resonator with liquid crystal cladding," *Opt Exp.*, vol. 24, no. 2, pp. 1002–1007, Jan. 2016.
[8] H. T. Kim and M. Yu, "Cascaded ring resonator-based temperature sensor with simultaneously enhanced sensitivity and range," *Opt. Exp.*, vol. 24, no. 9, pp. 9501–9510, May 2016.
[9] S. Saeedi and A. Emami, "Silicon-photonic PTAT temperature sensor for micro-ring resonator thermal stabilization," *Opt. Exp.*, vol. 23, no. 17, pp. 21875–21883, Aug. 2015.
[10] H. Yi, D. S. Citrin, and Z. Zhou, "Highly sensitive athermal optical microring sensor based on intensity detection," *IEEE J. Quantum Electron.*, vol. 47, no. 3, pp. 354–358, Mar. 2011.

[11] H. S. Lee, G. D. Kim, and S. S. Lee, "Temperature compensated refractometric biosensor exploiting ring resonators," *IEEE Photon. Technol. Lett.*, vol. 21, no. 16, pp. 1136–1136, Aug. 2009, Art. no. 1136.
[12] X. Zhang, X. Feng, D. Zhang, and Y. Huang, "Compact temperature - insensitive modulator based on a silicon microring assistant Mach-Zehnder interferometer," *Chin. Phys. B*, vol. 21, no. 12, pp. 250–257, 2012.
[13] B. Guha, B. B. C. Kyotoku, and M. Lipson, "CMOS-compatible athermal silicon microring resonators," *Opt. Exp.*, vol. 18, no. 4, pp. 3487–3493, Feb. 2010.
[14] Q. Deng, X. Li, Z. Zhou, and H. Yi, "Athermal scheme based on resonance splitting for silicon-on-insulator microring resonators," *Photon. Res.*, vol. 2, no. 2, pp. 71–74, Apr. 2014.
[15] R. Haldar, A. D. Banik, M. S. Sanathanan, and S. K. Varshney, "Compact athermal electro-optic modulator design based on SOI off-axis microring resonator," in *Proc. Conf. Lasers Electro-Opt., Appl. Technol.*, Jun. 2014, Paper JW2A.37.
[16] E. Timurdogan, C. M. Soraceagaskar, J. Sun, E. S. Hosseini, A. Biberman, and M. R. Watts, "An ultralow power athermal silicon modulator," *Nature Commun.*, vol. 5, no. 5, Jun. 2011, Art. no. 4008.
[17] B. Guha and M. Lipson, "Controlling thermo-optic response in microresonators using bimaterial cantilevers," *Opt. Lett.*, vol. 40, no. 1, pp. 103–106, Jan. 2015.
[18] S. Yokoyama, F. Qiu, Y. Feng, A. M. Spring, and K. Yamamoto, "0.018pm/°C Athermal silicon nitride ring resonator by polymer cladding," in *Proc. Conf. Lasers Electro-Opt./Pacific Rim*, Jul. 2013, Paper ThL2_4.
[19] L. He, Y. F. Xiao, C. Dong, and J. Zhu, "Compensation of thermal effect in high-Q toroidal microresonators by PDMS coating," in *Proc. Conf. Lasers Electro-Opt.*, Jun. 2009, Paper CTuE6.
[20] W. N. Ye, R. Sun, J. Michel, L. Eldada, D. Pant, and L. C. Kimerling, "Thermo-optical compensation in high-index-contrast waveguides," *Integr. Photon. Nanophoton. Res. Appl.*, Jul. 2008, Paper IWG3.
[21] J. Ptasinski, I. C. Khoo, and Y. Fainman, "Passive temperature stabilization of silicon photonic devices using liquid crystals," *Materials*, vol. 7, no. 3, pp. 2229–2241, Mar. 2014.
[22] N. Lin, L. Jiang, S. Wang, L. Yuan, and Q. Chen, "Simultaneous measurement of refractive index and temperature using a microring resonator," *Chin. Opt. Lett.*, vol. 10, no. 5, pp. 66–69, May 2012.
[23] P. Liu and Y. Shi, "Simultaneous measurement of refractive index and temperature using a dual polarization ring," *Appl. Opt.*, vol. 55, no. 13, pp. 3537–3541, May 2016.
[24] A. Arbabi and L. L. Goddard, "Measurements of the refractive indices and thermo-optic coefficients of Si_3N_4 and SiO_x using microring resonances," *Opt. Lett.*, vol. 38, no. 19, pp. 3878–3881, Oct. 2013.
[25] T. Wu, Y. Liu, Z. Yu, Y. Peng, C. Shu, and H. Ye, "The sensing characteristics of plasmonic waveguide with a ring resonator," *Opt. Exp.*, vol. 22, no. 7, pp. 7669–7677, Apr. 2014.
[26] R. W. Boyd and J. E. Heebner, "Sensitive disk resonator photonic biosensor," *Appl. Opt.*, vol. 40, no. 31, pp. 5742–5747, Nov. 2001.
[27] K. R. Hiremath, R. Stoffer, and M. Hammer, "Modeling of circular integrated optical microresonators by 2-D frequency domain coupled mode theory," *Opt. Commun.*, vol. 257, no. 2, pp. 277–297, Jan. 2006.
[28] E. F. Franchimon, K. R. Hiremath, R. Stoffer, and M. Hammer, "Interaction of whispering gallery modes in integrated optical microring or microdisk circuits: hybrid coupled mode theory model," *J. Opt. Soc. Amer. B*, vol. 30, no. 4, pp. 1048–1057, Apr. 2013.
[29] W. Bogaerts *et al.*, "Silicon microring resonators," *Laser Photon. Rev.*, vol. 6, no. 1, pp. 47–73, Sep. 2012.
[30] C. Ciminelli, C. M. Campanella, F. Dell Olio, C. E. Campanella, and M. N. Armenise, "Label-free optical resonant sensors for biochemical applications," *Prog. Quantum Electron.*, vol. 37, no. 2, pp. 51–107, Mar. 2013.
[31] A. Prinzen, M. Waldow, and H. Kurz, "Fabrication tolerances of SOI based directional couplers and ring resonators," *Opt. Exp.*, vol. 21, no. 14, pp. 17212–17220, Jul. 2013.
[32] M. Borselli, T. Johnson, and O. Painter, "Beyond the Rayleigh scattering limit in high-Q silicon microdisks: Theory and experiment," *Opt. Exp.*, vol. 13, no. 5, pp. 1515–1530, Mar. 2005.
[33] B. E. Little and S. T. Chu, "Estimating surface-roughness loss and output coupling in microdisk resonators," *Opt. Lett.*, vol. 21, no. 17, pp. 1930–1932, Sep. 1996.
[34] D. Lee, J. Bae, S. Hong, H. Yang, and Y. B. Kim, "Optimized antireflective silicon nanostructure arrays using nanosphere lithography," *Nanotechnology*, vol. 27, no. 21, May 2016, Art. no. 215302.
[35] I. M. White and X. Fan, "On the performance quantification of resonant refractive index sensors," *Opt. Exp.*, vol. 16, no. 2, pp. 1020–1028, Jan. 2008.
[36] S. T. Fard *et al.*, "Performance of ultra-thin SOI-based resonators for sensing applications," *Opt Exp.*, vol. 22, no. 12, pp. 14166–14179, Jun. 2014.
[37] V. V. Tuchin, I. L. Maksimova, D. A. Zimnyakov, I. L. Kon, A. H. Mavlyutov, and A. A. Mishin, "Light propagation in tissues with controlled optical properties," *J. Biomed. Opt.*, vol. 2, no. 4, pp. 401–417, Oct. 1997.
[38] X. Fan, I. M. White, H. Zhu, and J. D. Suter, "Overview of novel integrated optical ring resonator bio/chemical sensors," in *Proc SPIE Laser Resonators Beam Control IX*, Feb. 2007, paper 64520M.
[39] T. Ma *et al.*, "Integrated label-free optical biochemical sensor with a large measurement range based on an angular grating-microring resonator," *Appl. Opt.*, vol. 55, no. 18, pp. 4784–4790, Jun. 2016.
[40] S. Selvaraja *et al.*, "Highly uniform and low-loss passive silicon photonics devices using a 300 mm CMOS platform," in *Proc. Opt. Fiber Commun. Conf.*, 2014, paper Th2A.33.